Volume 10 | Number 14 | 21 July 2023

10 YEARS ANNIVERSARY

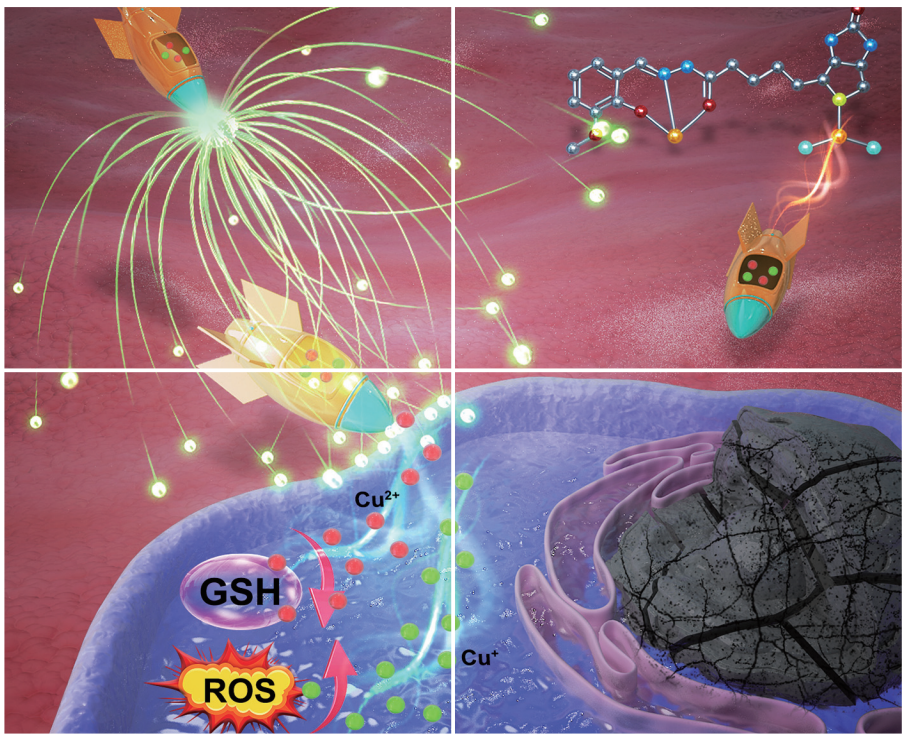

INORGANIC CHEMISTRY

FRONTIERS

CCS 中国化学会 CHINESE CHEMICAL SOCIETY
PEKING UNIVERSITY 1898
ROYAL SOCIETY OF CHEMISTRY
rsc.li/frontiers-inorganic

INORGANIC CHEMISTRY FRONTIERS

RESEARCH ARTICLE

View Article Online
View Journal | View Issue

Cite this: *Inorg. Chem. Front.*, 2023, **10**, 4045

A mixed-valence biotinylated Cu(I/II) complex for tumor-targeted chemodynamic therapy accompanied by GSH depletion†

Zhaoguo Hong, Xin You, Jingjing Zhong, Di Yao, He-Dong Bian, Shulin Zhao, Liangliang Zhang,* Hong Liang* and Fu-Ping Huang*

Chemodynamic therapy (CDT), in which highly toxic hydroxyl radicals (˙OH) could be triggered by a Fenton or Fenton-like reaction to kill cancer cells, has emerged recently. Compared to traditional CDT nanomaterials, herein, an atomically-precise biotinylated Cu(I/II) complex $[Cu^{I}Cu^{II}Cl_2(VBio)]\cdot CH_3OH$ (VBio = deprotonated *O*-vanillin biotinylhydrazone), denoted **VBio-Cu^{I}Cu^{II}**, was rationally designed and synthesized successfully. This targeted Fenton-like agent, **VBio-Cu^{I}Cu^{II}**, is constructed from a hydroxyl radical-producible Cu^{I} ion, a Cu^{II} center as a GSH depletor for an augmented CDT effect, and a biotin moiety as a cancer-targeting unit. Owing to the obvious cell selectivity discrepancy of biotin towards normal and cancerous cells, **VBio-Cu^{I}Cu^{II}** was able to preferentially accumulate in tumor cells. Meanwhile, the Cu^{I} metal center could be used as a Fenton-like agent to generate ˙OH. Furthermore, the Cu^{II} in **VBio-Cu^{I}Cu^{II}** was available for successive ˙OH production *via* a Cu^{I}/Cu^{II}-circulation strategy under a GSH-rich tumor site, thereby improving catalytic efficiency. More importantly, *in vivo* results further demonstrate that **VBio-Cu^{I}Cu^{II}** could significantly inhibit tumor growth without obvious damage toward major organs. Therefore, this multiple-identity Fenton-like agent could provide an appreciable reference value for the design of atomically precise CDT agents.

Received 10th February 2023,
Accepted 31st March 2023

DOI: 10.1039/d3qi00254c

rsc.li/frontiers-inorganic

Introduction

Chemodynamic therapy (CDT), which is based on overproduced hydrogen peroxide (H_2O_2)[1] in a tumor that can generate cytotoxic hydroxyl radicals (˙OH) by Fenton or Fenton-like reactions, has emerged as a new and novel therapeutic approach.[2,3] In particular, ˙OH could damage various biomolecules (such as nucleic acids, proteins and lipids) and further induce cell death.[4–6] Nowadays, Fenton/Fenton-like nano-catalysts based on Fe, Mn, Cu, *etc*. have been explored as CDT agents and have shown considerable therapeutic efficiency.[7–9] Despite many examples of excellent performance of CDT in cancer treatment, its therapeutic efficacy is commonly limited by the low and heterogeneous distribution of H_2O_2 concentration (50–100 μM) inside the tumor region, although H_2O_2 overproduction is one of the hallmarks of tumors compared with normal tissues.[10,11] Moreover, the upregulated antioxidant defense in a tumor (like overproduced glutathione, GSH, of up to 10×10^{-3} M, about four-fold that of normal cells, which could scavenge ˙OH) also compromises the treatment efficiency of CDT.[12,13]

To circumvent these difficulties, many attempted solutions have been proposed. On the one hand, researchers have focused on a Cu(I)-based Fenton-like reaction, which shows better efficiency than an Fe-based Fenton reaction in weakly acidic or neutral media.[14,15] On the other hand, to disrupt the antioxidant defense system of the tumor, GSH-depletion has been employed as an effective strategy in CDT.[16,17] Furthermore, sufficient tumor cell selectivity is another attractive issue, which is still challenging for the most commonly reported CDT agents.[18,19] Tumor selectivity is definitely important for CDT, which can reduce side effects. It is well established that introducing high-affinity ligands with cell-specific recognition to deliver therapeutic agents into a tumor site is an effective way to enhance selectivity.[20,21] Our group focuses on developing atomically-precise metal complexes with Fenton/Fenton-like catalytic ability as CDT agents. In previous work, we prepared a feasible biotinylated Cu(I) complex for tumor-targeted CDT,[22] in which biotin was employed as a tumor-targeting ligand for receptor-mediated drug delivery.[23–26] We considered that the efficiency of a single-

State Key Laboratory for Chemistry and Molecular Engineering of Medicinal Resources, School of Chemistry and Pharmaceutical Sciences, Guangxi Normal University, Guilin, 541004, China. E-mail: liangzhang319@163.com, hliang@mailbox.gxnu.edu.cn, huangfp2010@163.com

†Electronic supplementary information (ESI) available. CCDC 2218318 and 2218319. For ESI and crystallographic data in CIF or other electronic format see DOI: https://doi.org/10.1039/d3qi00254c

valence Cu(I)-based CDT agent might be compromised by the disorder of antioxidant defense. Therefore, multifunctional tumor-targeted CDT agents integrated with effective ˙OH production and GSH-depletion functions are highly desirable for effective CDT. Although nanomedicine based on biotin-targeted tumor therapy has been reported yet, atomically-precise biotinylated metal complexes have been rarely reported due to the difficulty of crystallization caused by the present of the *C*4 chain in biotin structure.

Benefiting from their precise formulas, both the structure and the catalytic properties of atomically precise CDT agents are easily repeated and controllable. Herein, an *O*-vanillin biotinylhydrazone (denoted HVBio) ligand was synthesized, in which the acylhydrazone group and the sulfur atom in biotin are conducive to the coordination of divalent copper and monovalent copper, respectively. Subsequently, a biotinylated mixed-valence (both monovalent and divalent) copper complex $[Cu^{I}Cu^{II}Cl_2(VBio)]\cdot CH_3OH$ (**VBio-Cu^{I}Cu^{II}**) was rationally constructed as a multifunctional CDT agent with effective ˙OH production, GSH-depletion and biotin-guided tumor-targeting (Scheme 1). The biotin here can offer good targeting to its receptor-positive cancer cells. In addition, Cu(I) in this complex can react with H_2O_2 to generate hypertoxic ˙OH directly through the Fenton-like reaction. What is more, GSH depletion can be achieved by the incorporated Cu(II) accompanied by the production of Cu(I), and the new product Cu(I) will undergo further catalytic reaction to generate more ˙OH. So, we think that such a Cu(I/II) complex, **VBio-Cu^{I}Cu^{II}**, has better catalytic performance in the tumor site due to the overproduction of GSH and H_2O_2. Obviously, the prepared biotinylated Cu(I/II) mixed-valence complex **VBio-Cu^{I}Cu^{II}** with tumor-targeting, Cu(I)-catalysed Fenton-like reaction and Cu(II)-assisted GSH depletion exhibits improved therapeutic efficiency through the synergism effect, which provides a new opportunity for constructing enhanced targeted CDT agents with atomically precise structure.

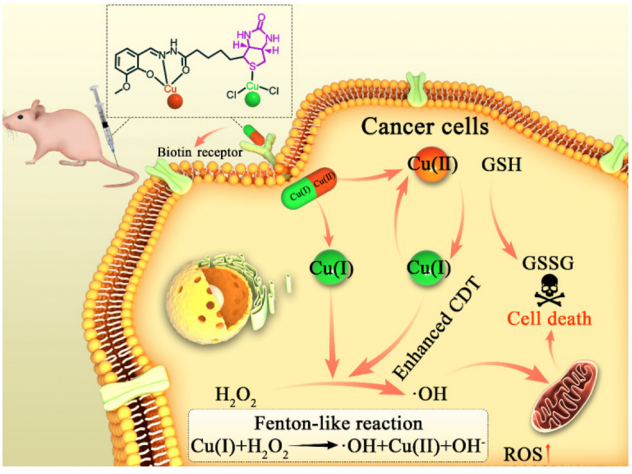

Scheme 1 Schematic illustration of **VBio-Cu^{I}Cu^{II}** for enhanced CDT therapy.

Results and discussion

Synthesis and characterization

In this study, the ligand *O*-vanillin biotinylhydrazone was prepared first through a classical Schiff base condensation using *O*-vanillin and biotin hydrazide under reflux in ethanol. Then, **VBio-Cu^{I}Cu^{II}** was obtained using the corresponding ligand HVBio (1 equiv.) with $CuCl_2\cdot 2H_2O$ (2 equiv.), as shown in Scheme S1.† The crystal was obtained by a solution method and measured using single-crystal X-ray crystallography. Crystallographic parameters, selected bond distances and angles are summarized in Tables S1–S2,† respectively. The penta-coordinated Cu^{II} (Cu1) center in distorted square pyramidal geometry was coordinated by the 'ONO' tridentate Schiff base ligand of HVBio and one methanol molecule, accompanied by a carbonyl oxygen atom (O1A, symmetric code: A: $1-x$, $-0.5+y$, $1-z$) of biotin (Fig. 1a and Fig. S1a†). The Cu^{I} (Cu2) center is coordinated by two chlorine atoms and one sulfur atom (from the thiophene ring of biotin) to form trigonal geometry in **VBio-Cu^{I}Cu^{II}**; the Cu2–Cl1 and Cu2–Cl2 distances are 2.221(4) Å and 2.260(3) Å, respectively, and the Cu2–S1 distance is 2.235(3) Å. The carbonyl oxygen atom of the biotin bridge is adjacent to Cu(II) centers, leading to a 1D chain. Furthermore, the valence state analysis of **VBio-Cu^{I}Cu^{II}** was determined by X-ray photoelectron spectroscopy (XPS, Fig. 1b), which exhibits Cu 2p3/2 and Cu 2p1/2 peaks at 932.3 and 952.4 eV, respectively, with peaks shifting to higher binding energies at 933.8 and 954.2 eV, suggesting the co-existence of Cu(I) and Cu(II) in **VBio-Cu^{I}Cu^{II}**.[27,28] Meanwhile, as a control, we also prepared a single-valence Cu(II) complex **VBio-Cu^{II}**, which was obtained by the reaction of HVBio and $Cu(NO_3)_2\cdot 3H_2O$ (Scheme S1†). The crystal structure, crystallographic information, and XPS characterization of **VBio-Cu^{II}** are given in Fig. S1, S2 and Tables S1, S2.† On the other hand, the phase purity of the two complexes was investigated by powder X-ray diffraction (PXRD). All PXRD patterns of the two complexes corresponded well with the simulated patterns calculated from the single-crystal X-ray diffraction data (Fig. S3†), which suggested good purity, and from the HPLC spectra results they both exhibit good stability in PBS over 48 h (Fig. S4†).

Fenton-like catalytic performances of VBio-Cu^{I}Cu^{II}

It is well known that Cu(I) could catalyse the decomposition of H_2O_2 to generate ˙OH by a Fenton-like reaction.[29,30] Here, methylene blue (MB) was used as a colorimetric indicator to

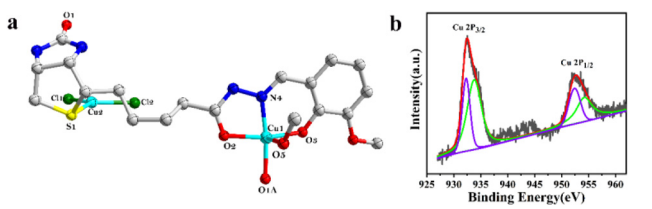

Fig. 1 (a) Crystal structure of **VBio-CuICuII** (anions, hydrogen atoms and solvent molecules are omitted for clarity). (b) XPS spectra of **VBio-CuICuII**.

study the generation of ˙OH catalysed by **VBio-Cu^{I}Cu^{II}**. As shown in Fig. 2a, compared to MB or MB + H_2O_2 groups, the absorbance of MB was reduced accompanied by color fading after it reacted with **VBio-Cu^{I}Cu^{II}** in the presence of H_2O_2, indicating that there was a degradation in MB. As expected, with further addition of GSH (10 mM) into the **VBio-Cu^{I}Cu^{II}** + H_2O_2 catalysis system, a greater decrease in absorbance was observed and the MB solution underwent intuitive fading to colorless. In addition, the degree of MB fading was enhanced with an increase in GSH concentration (Fig. 2b). Meanwhile, we also employed electron paramagnetic resonance (EPR) spectra to investigate ˙OH generation using 5,5-dimethyl-1-pyrroline *N*-oxide (DMPO) as an ˙OH trapping agent. As shown in Fig. 2c, the characteristic 1 : 2 : 2 : 1 signal of ˙OH was observed for the **VBio-Cu^{I}Cu^{II}** + H_2O_2 group, owing to the existence of Cu(I) in **VBio-Cu^{I}Cu^{II}** that can catalyse ˙OH production by a Fenton-like reaction. Similar to the MB degradation experiment, after adding GSH into a **VBio-Cu^{I}Cu^{II}** solution with H_2O_2, stronger characteristic signal peaks appeared. The increase in ˙OH signal was attributed to the GSH-catalysed reduction of Cu(II) in **VBio-Cu^{I}Cu^{II}**, generating more Cu(I) for an enhanced Fenton-like reaction.[31,32] To demonstrate this, the single-valence control complex **VBio-Cu^{II}** was introduced to react with GSH in the presence of H_2O_2. As can be seen in Fig. 2c, the ˙OH signal was also obtained from the **VBio-Cu^{II}** + H_2O_2 + GSH group but with a lower intensity compared with that from the **VBio-Cu^{I}Cu^{II}** + H_2O_2 + GSH group. Therefore, the above results showed that the rationally designed Cu(I/II) mixed-valence complex **VBio-Cu^{I}Cu^{II}** can act as a Cu(I)-based Fenton reagent to catalyse the generation of ˙OH, and GSH promotes this reaction through the GSH-induced reduction of Cu(II) in **VBio-Cu^{I}Cu^{II}** to produce new Cu(I).

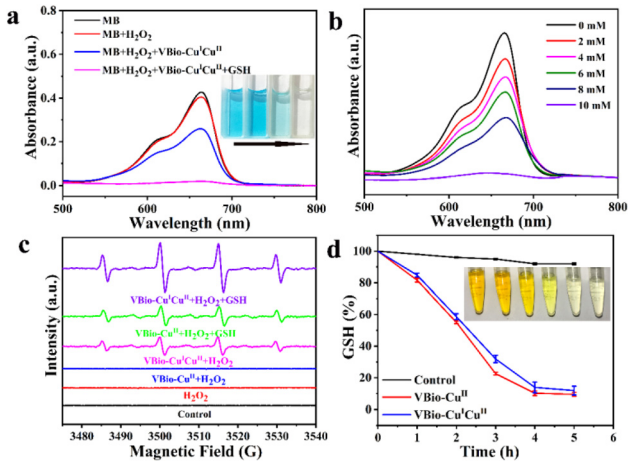

Fig. 2 (a) UV-vis absorption spectra of MB under different conditions. Inset: the corresponding photographs of MB solutions. (b) MB degradation test in the presence of GSH with different concentrations from 0 to 10 mM. (c) EPR spectra of different testing groups. (d) GSH (10 mM) depletion by **VBio-Cu^{I}Cu^{II}** and **VBio-Cu^{II}** (10 mM) at 37 °C for 0 to 5 h, respectively. Inset: the corresponding photographs of DTNB solutions treated with **VBio-Cu^{I}Cu^{II}** for different incubation times (from left to right: 0, 1, 2, 3, 4, and 5 h).

GSH depletion

The accompanying GSH depletion during the reduction of Cu(II) was also monitored using 5,5′-dithiobis-(2-nitrobenzoic acid) (DTNB) as an indicator, which could react with GSH to form a yellow 5-thio-2-nitrobenzoic acid.[33] After co-incubation with **VBio-Cu^{I}Cu^{II}**, the level of GSH in aqueous solution (containing 10% DMF) exhibited sustained reduction within 6 h (Fig. 2d), which is similar to that for single-valence control complex **VBio-Cu^{II}**, indicating that GSH could be consumed in the presence of **VBio-Cu^{I}Cu^{II}**. Furthermore, we collected the supernatant for a high resolution mass spectrometry (HR-MS) test. From the HR-MS result (Fig. S5a–5d†), a strong MS peak at ~613 *m*/*z* was observed after adding **VBio-Cu^{I}Cu^{II}** into GSH solution, and the isotope distributions closely matched the simulated patterns of GSSG, which is the oxidation product of GSH. All these results demonstrated that GSH could be consumed by **VBio-Cu^{I}Cu^{II}** through the GSH-catalysed reduction of Cu(II) in **VBio-Cu^{I}Cu^{II}**.

In vitro cytotoxicity and cellular uptake

Taking advantage of the effective ˙OH generation and GSH depletion capacity of **VBio-Cu^{I}Cu^{II}**, the prepared mixed-valence Cu(I/II) complex can serve as a CDT agent. So, the potential cytotoxicity of **VBio-Cu^{I}Cu^{II}** was evaluated first according to the standard MTT assay. Murine breast cancer 4T1 cells (biotin receptor-positive) were treated with varying concentrations of **VBio-Cu^{I}Cu^{II}** for 48 h. As shown in Fig. 3a, the cell viability measurements for **VBio-Cu^{I}Cu^{II}** against 4T1 cells showed a dose-dependent relationship. Only about 28.1% of cells were alive after the treatment with **VBio-Cu^{I}Cu^{II}** at 25 μM. The decrease in cell viability was attributed to the conversion of intracellular overproduced H_2O_2 to ˙OH by a **VBio-Cu^{I}Cu^{II}**-mediated Fenton-like reaction that induced the killing of cells. Compared to the decrease produced by solely adding **VBio-Cu^{I}Cu^{II}**, it is worth noting that, when adding exogenous H_2O_2, the cell viability markedly decreased due to the generation of more highly toxic ˙OH from exogenous H_2O_2. Moreover, as shown in Fig. 3b, no obvious toxicity of **VBio-Cu^{I}Cu^{II}** to human embryo lung fibroblast WI38 cells (biotin receptor-negative) was observed and the cell viability was maintained above 80% even in the presence of exogenous H_2O_2. This implied that the prepared **VBio-Cu^{I}Cu^{II}** can kill cancer cells *via* CDT and shows potential to target biotin receptor-positive cells. It is undeniable that the introduction of targeting-group biotin here could improve targeting ability through receptor-mediated endocytosis, resulting in minimal damage to normal cells in CDT.[34,35] Subsequently, the cell apoptosis caused by **VBio-Cu^{I}Cu^{II}** was further investigated by flow cytometry. The ratio of apoptotic cells increased significantly when 4T1 cells were incubated with **VBio-Cu^{I}Cu^{II}** (25 μM), while the **VBio-Cu^{II}**-treated 4T1 cells showed only a moderate apoptotic rate (Fig. 3c). This demonstrated that the dual-valence Cu(I/II) complex had much better anticancer ability than a single-valence Cu(II) complex. Likewise, the apoptosis results (Fig. 3d) towards WI38 cells show that both **VBio-Cu^{I}Cu^{II}** and **VBio-Cu^{II}** had a much lower

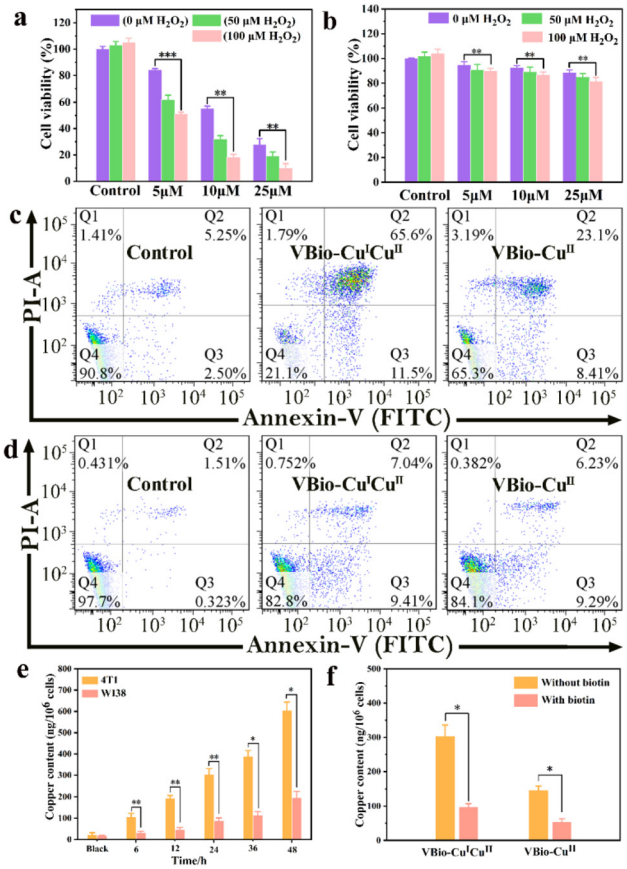

Fig. 3 Relative viabilities of 4T1 (a) and WI38 (b) cells after incubating with **VBio-Cu^{I}Cu^{II}** in the presence or absence of H_2O_2 for 48 h. Flow cytometry assay of 4T1 (c) and WI38 (d) cells after treatments with **VBio-Cu^{I}Cu^{II}** or **VBio-Cu^{II}** (25 μM) for 48 h. (e) The intracellular Cu content in 4T1 and WI38 cells after treatment with **VBio-Cu^{I}Cu^{II}**. (f) The intracellular Cu content in 4T1 cells pre-treated with or without 10 μg mL^{-1} biotin followed by incubation with 10 μM **VBio-Cu^{I}Cu^{II}** or **VBio-Cu^{II}** for 24 h.

killing effect on biotin receptor-negative cells, further indicating their targeting ability.

To gain an insight into the different targeting performance of **VBio-Cu^{I}Cu^{II}** towards 4T1 and WI38 cells, the cellular uptake of **VBio-Cu^{I}Cu^{II}** was then studied by determining intracellular Cu using inductively coupled plasma mass spectrometry (ICP-MS). The results in Fig. 3e showed that the contents of intracellular Cu both in 4T1 and in WI38 cells were increased with the increase in incubation time of **VBio-Cu^{I}Cu^{II}**, but more intracellular Cu was obtained in 4T1 cells than that in WI38 cells. This indicated that **VBio-Cu^{I}Cu^{II}** preferred to accumulate in 4T1 cells, thereby exerting a good targeted CDT. The selective accumulation originated from the biotin receptor-mediated delivery of biotinylated **VBio-Cu^{I}Cu^{II}**. To further prove the existence of ligand–receptor interactions, competitive uptake of biotinylated complex into 4T1 cells was carried out in the presence of free biotin. As shown in Fig. 3f, for both **VBio-Cu^{I}Cu^{II}** and **VBio-Cu^{II}**, the intracellular Cu contents were markedly decreased when 4T1 cells were pre-treated with free biotin followed by the incubation of biotinylated complexes. The free biotin molecules competitively combined with the biotin receptors on the surface of 4T1 cells, which hampered the binding between biotinylated complexes and biotin receptors, suggesting that the biotin–receptor interaction was crucial for the cancer-targeting ability of **VBio-Cu^{I}Cu^{II}**. Moreover, a biotin-free copper complex (Fig. S6,† denoted **VBh-Cu^{II}**) was obtained by the reaction of *O*-vanillin benzoylhydrazone with copper chloride; however, **VBh-Cu^{II}** showed indiscriminate cytotoxicity towards 4T1 and WI38 cells (Fig. S6†), further confirming that the biotin group is conducive to the construction of targeted drugs.

Intracellular GSH depletion and ROS generation

In vitro experiments have demonstrated that **VBio-Cu^{I}Cu^{II}** held great potential as an effective CDT agent, because of the effective production of ˙OH and the consumption of GSH. Then, the intracellular performances of **VBio-Cu^{I}Cu^{II}** for GSH depletion and ROS generation were also explored. After 4T1 cells were treated with **VBio-Cu^{I}Cu^{II}** or **VBio-Cu^{II}**, the cell supernatant obtained by repeated freeze–thaw lysis was further determined using a GSH/GSSG assay kit. And the intracellular GSH/GSSG ratio of 4T1 cells was decreased (Fig. 4a). This indicated that the depletion of GSH occurred in 4T1 cells, which could further enhance CDT efficiency. After that, since CDT relied on the generation of ˙OH, the change in intracellular ROS was evaluated by a flow cytometry assay using 2,7′-dichlorodihydrofluorescein diacetate (DCFH-DA) as the ROS indicator, to demonstrate the **VBio-Cu^{I}Cu^{II}**-induced generation of ROS in cells. As presented in Fig. 4b, compared with the control group, a shift in flow cytometry results was observed in the complex-treated cells, indicating the generation of ROS after the incubation of a copper complex with cells. At the same time, we found that the shift of **VBio-Cu^{I}Cu^{II}**-treated cells was larger than that of **VBio-Cu^{II}**-treated cells, proving that more ROS was produced in the **VBio-Cu^{I}Cu^{II}**-treated cells. Therefore, these results clearly and intuitively showed that the prepared **VBio-Cu^{I}Cu^{II}** could produce ROS effectively in cells with the consumption of intracellular GSH, enabling higher cancer cell killing ability.

In vivo tumor therapy performance

The *in vivo* application of a **VBio-Cu^{I}Cu^{II}** for an antitumor effect was then evaluated in 4T1 cell-xenograft tumor-bearing

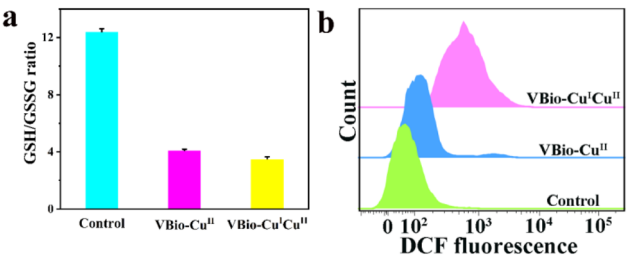

Fig. 4 (a) The intracellular GSH/GSSG ratios in 4T1 cells treated with **VBio-Cu^{I}Cu^{II}** or **VBio-Cu^{II}** for 12 h. (b) Intracellular ROS detection in 4T1 cells using flow cytometry.

mice. The mice were divided randomly into three groups: saline-treated control group, **VBio-Cu^{II}**-treated group, and **VBio-Cu^{I}Cu^{II}**-treated group. Different agents (saline, **VBio-Cu^{II}** and **VBio-Cu^{I}Cu^{II}**) were intravenously injected into tumor-bearing mice every other day. During the treatment, the body weight and tumor volume of each mouse were monitored every other day. As can be seen from Fig. 5a, the animal weights of all tested groups increased slightly without obvious loss during the treatments. At the same time, the tumor volume increased gradually in the control group, and the copper-complex-treated groups showed a lower rate of increase (Fig. 5b), demonstrating the inhibition effect of the copper complex on tumor growth. The excised tumors from each group also confirmed the therapeutic efficiency (Fig. 5c). What is more, similar to the results shown in the *in vitro* cytotoxicity results, **VBio-Cu^{I}Cu^{II}** shows a much stronger tumor inhibition effect with much smaller tumor size than **VBio-Cu^{II}** (Fig. 5b and c). This indicated that Cu(I/II) mixed-valence **VBio-Cu^{I}Cu^{II}** could indeed achieve an enhanced CDT with excellent therapeutic performance. Finally, the biosafety of **VBio-Cu^{I}Cu^{II}** *in vivo* was also tested using an H&E (hematoxylin and eosin) staining assay on the major organs (including heart, liver, spleen, lung, and kidney) after treatment (Fig. 5d). The results showed that **VBio-Cu^{I}Cu^{II}** and **VBio-Cu^{II}** did not induce a remarkable difference in physiological morphology after administration, which further illustrated good *in vivo* biocompatibility. Based on the above results, the prepared **VBio-Cu^{I}Cu^{II}** could effectively inhibit the tumor as a CDT agent with low side effects.

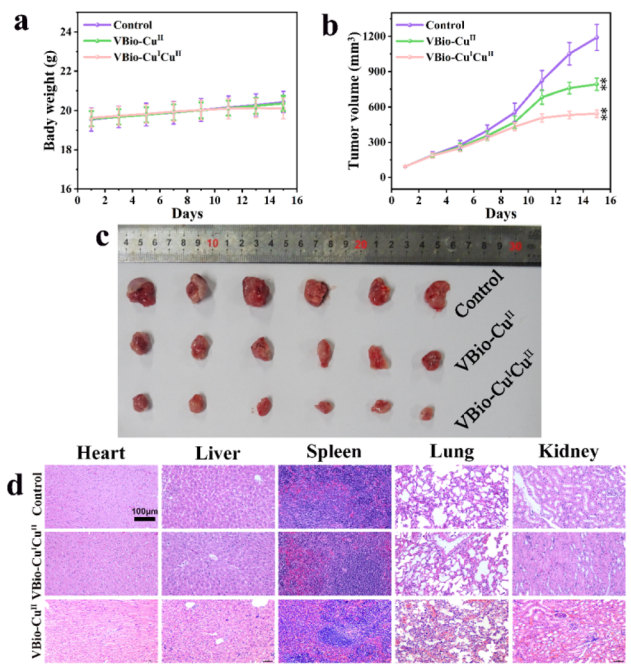

Fig. 5 The changes in body weight (a) and tumor volume (b) during the treatments. (c) The photographs of the excised tumors after different treatments. Stripped tumors after treatment with **VBio-Cu^{II}** (20 mg kg^{-1}) or **VBio-Cu^{I}Cu^{II}** (20 mg kg^{-1}). (d) Histological slices obtained from main tissues (heart, liver, spleen, lung, and kidney) of mice after treatment. Scale bar: 100 μm.

Conclusions

In summary, a biotinylated Cu(I/II) mixed-valence complex **VBio-Cu^{I}Cu^{II}** was rationally designed and prepared here for enhanced CDT. **VBio-Cu^{I}Cu^{II}** showed good targeting ability for biotin–receptor-positive cancer cells. Cu(I) in **VBio-Cu^{I}Cu^{II}** can react with endogenous H_2O_2 to generate hypertoxic $^{\bullet}OH$ directly. Simultaneously, GSH depletion can be achieved by the incorporated Cu(II) accompanied by the production of Cu(I), which further increases the amount of $^{\bullet}OH$. The "three in one" construction motivates the potential of each component in response to the tumor microenvironment. Thus, our rational design strategy provides a novel approach for the development of tumor-targeting and enhanced CDT based on atomically precise metal complexes, and further expands the chemical space for the design of multifunctional CDT agents.

Experimental

Materials and instruments

All reagents and solvents were obtained from commercial suppliers and used without further purification. Biotin hydrazide, *O*-vanillin, $Cu(NO_3)_2{\cdot}3H_2O$, $CuCl_2{\cdot}2H_2O$, 5,5-dimethyl-1-pyrroline-*N*-oxide (DMPO), 5,5′-dithiobis(2-nitrobenzoic acid) (DTNB), and methylene blue (MB) were provided by Aladdin (Shanghai, China). 3-(4,5-Dimethylthiazol-2-yl)-2,5-diphenyltetrazolium bromide (MTT), 2,7′-dichlorodihydrofluorescein diacetate (DCFH-DA), and Annexin V-FITC/propidium iodide (PI) staining agents were purchased from Beyotime (Shanghai, China). GSH and GSSG assay kits were purchased from Solarbio (Beijing, China). All cells were obtained directly from the cell bank of Shanghai Institute of Life Sciences (China) and cultured in Roswell Park Memorial Institute (RPMI) 1640 medium or Dulbecco's modified Eagle medium (DMEM) containing 10% FBS (Gibco). The single-crystal structures of the complexes were measured on an Agilent Technologies SuperNova diffractometer using Mo-Kα radiation (λ = 0.71073 Å) at 293 K. High resolution mass spectrometric data were recorded using a Q Exactive mass spectrometer (Thermo Scientific). Infrared spectra were recorded on KBr pellets using a Spectrum Two FTIR spectrometer (PerkinElmer Inc., USA). C and H analyses were determined using a Vario EL III Cube elemental analyzer. UV-vis spectra were recorded on a Cary 60 spectrometer. Electron paramagnetic resonance (EPR) spectra were recorded on a Bruker EMX1598 spectrometer. X-ray photoelectron spectroscopy (XPS) analysis was performed on a Thermo NEXSA spectrometer equipped with a monochromatic Al Kα X-ray source (1486.6 eV) operated at 15 kV and 150 W and a hemispherical energy analyzer. The inductively coupled plasma mass spectrometry (ICP-MS) data were obtained on a FLexar-NexION300X ICP-MS instrument (PerkinElmer Inc.,

USA). Flow cytometry experiments were performed on a FACS Aria II flow cytometry instrument (BD Biosciences, San Jose, USA).

Synthesis of VBio-Cu^{I}Cu^{II} and VBio-Cu^{II}

Briefly, biotin hydrazide was treated with an equivalent of *O*-vanillin through condensation in EtOH at 80 °C, yielding ligand *O*-vanillin biotinylhydrazone (HVBio). Anal. Calc. (%) for $C_{18}H_{24}N_4O_4S$: C, 55.08; H, 6.12; N, 14.28. Found: C, 54.92; H, 6.00; N, 14.47. HR-MS (ESI): *m*/*z* = 393.1599 [HVBio + H]$^+$, IR (KBr, cm^{-1}): 3943 w, 3791 m, 3378 s, 3283 w, 2928 m, 1678 vs, 1452 s, 1258 s, 1149 w, 1079 w, 982 w, 752 m, 611 w. Subsequently, a methanolic solution of HVBio (0.1176 g; 0.3 mmol; 10 mL) was refluxed until dissolved. A methanolic solution of excess $CuCl_2{\cdot}2H_2O$ (0.1023 g; 0.6 mmol; 10 mL) was then added and the resulting reaction mixture was stirred at 60 °C for 1 h. A blackish green solution was then cooled at room temperature with the slow evaporation of solvent to obtain a greenish-yellow block crystal of **VBio-Cu^{I}Cu^{II}**. Then, after washing with ethanol, **VBio-Cu^{I}Cu^{II}** was dried in air (yield: 48%). Anal. Calc. (%) for $C_{19}H_{27}Cl_2Cu_2N_4O_5S$: C, 36.68; H, 4.34; N, 9.01. Found: C, 36.55; H, 4.57; N, 8.90. HR-MS (ESI): *m*/*z* = 515.9932 [Cu^{I}Cu^{II} + VBio]$^+$ (Fig. S7a and b†), IR (KBr, cm^{-1}): 3195 m, 2933 m, 2842 w, 1664 vs, 1564 vs, 1446 s, 1230 m, 1232 s, 1096 w, 863 w, 724 s, 599 w.

VBio-Cu^{II} was obtained by a similar method to that described for the preparation of **VBio-Cu^{I}Cu^{II}** using $Cu(NO_3)_2{\cdot}3H_2O$ (0.056 g, 0.3 mmol) and HVBio. Dark green block crystals were obtained (yield: 81.1%). Anal. Calc. (%) for $C_{19}H_{28}CuN_5O_9S$: C, 40.28; H, 4.95; N, 12.37. Found: C, 39.93; H, 5.11; N, 12.14. HR-MS (ESI): *m*/*z* = 454.0687 [Cu + VBio]$^+$, (Fig. S7c and d†) IR (KBr, cm^{-1}): 3781 m, 3419 w, 3233 m, 2932 s, 1651 vs, 1566 vs, 1385 s, 1306 s, 1131 w, 1017 w, 814 m, 728 w, 634 w, 514 w. In this study, we also attempted to synthesize copper complexes using various anions (Cl^-, NO_3^-, ClO_4^-, SO_4^{2-}, Ac^-), molar ratios (1 : 1, 1 : 2, 1 : 3, 2 : 1, 3 : 1) and solvents (MeOH, EtOH, CH_2Cl_2, $CHCl_3$ *etc.*). However, crystalline samples of the complexes can be easily obtained in the presence of $CuCl_2$ or $Cu(NO_3)_2$. In particular, the reaction of $CuCl_2$ with ligands at a molar ratio of 2 : 1 can obtain Cu^{I}Cu^{II} crystalline complexes with higher yield compared to a 1 : 1 ratio. Overall, the counterion and stoichiometric ratio play an important role in coordination and crystallization.

Crystal structure determination and refinement

Single crystals of the two copper complexes were obtained at room temperature with graphite monochromatic Mo-Kα radiation (λ = 0.71073 Å). All structures were solved by a direct method by ShelXT[36] in the OLEX 2 program package,[37] and all non-hydrogen atoms were refined anisotropically by the full-matrix least-squares method on F^2 by using the SHELXL-2018 program package.[38] The parameters used intensity collection and refinements are summarized in Table S1,† and selected bond lengths and angles are given in Table S2.† Crystallographic data were deposited at the Cambridge Crystallographic Data Centre, CCDC 2218318 and 2218319.†

Stability test of complex

The stability of the two copper complexes (2×10^{-4} M) was monitored by HPLC (Waters e2695, Column: InertSustain C18, 2998 PDA Detector HPLC COLUMN, 150 mm × 5.0 μm, I.D.) after incubating in PBS (pH = 7.4) for different times. The mobile phase was methanol/water (9 : 1) containing 0.01% TFA. The wavelength was 200–400 nm. The flow rate was 0.65 mL min^{-1}. Samples (10 μL) were injected into the HPLC system at different time points.

Methylene blue (MB) degradation test

Firstly, MB aqueous solution (5 μM) was added into H_2O_2 (10 mM)-containing PBS (25 mM, pH = 7.4). Then 200 μM of freshly prepared **VBio-Cu^{I}Cu^{II}** was added into the above mixture with or without GSH (10 mM). The obtained solutions were then incubated for 12 h at 37 °C, and the absorption spectra were monitored by UV-vis spectroscopy.

Detection of $^{\cdot}$OH

EPR spectroscopy was used to detect the $^{\cdot}$OH generated in this work. In brief, the complex **VBio-Cu^{I}Cu^{II}** or **VBio-Cu^{II}** (200 μM) was incubated with or without GSH (10 mM) for 0.5 h. After that, H_2O_2 (100 mM) and DMPO (25 mM) were added into the above mixture. The $^{\cdot}$OH signal was determined with an EPR spectrometer.

GSH depletion assay

GSH depletion was determined using Ellman's assay. Briefly, solutions with 10 mM GSH and 50 μM **VBio-Cu^{I}Cu^{II}** or **VBio-Cu^{II}** were incubated at 37 °C for 0–5 h. Then, 10 mM DTNB solution was added to the mixed solutions and co-incubated for 10 min at room temperature. Afterward, the absorbance with the characteristic peak at 450 nm was measured with a microplate reader. For intracellular GSH consumption assay, 4T1 cells were seeded in 6-well plates at 1×10^5 cells per well and incubated overnight. Then, the cells were treated with **VBio-Cu^{I}Cu^{II}** or **VBio-Cu^{II}** (10 μM) for another 12 h. After that, the cells were collected before lysis by three freeze–thaw cycles. The supernatant was then collected and used for a GSH depletion assay in accordance with the operating instructions of the commercial GSH and GSSG assay kits.

Cytotoxicity assay

The cytotoxicity of the prepared complexes towards 4T1 and WI38 cells was first detected by an MTT method. Briefly, 4T1 and WI38 cells were seeded in a 96-well plate at a density of 1×10^4 cells per well, respectively. The complex (**VBio-Cu^{I}Cu^{II}** or **VBio-Cu^{II}**) with different concentrations (0, 5, 10 and 25 μM) was added to the cells with or without H_2O_2 followed by incubation for 48 h. Then, 10 μL MTT (5 mg mL^{-1}) solutions were added to each well. After 5 h of incubation, 100 μL of DMSO was added to dissolve the formazan crystals. Absorbance of the

solution from each well was measured at 570 nm. Cell viability was calculated with the following formula:

$$\text{Cell viability (\%)} = (\text{OD}_{\text{sample}} - \text{OD}_{\text{blank control}}) / (\text{OD}_{\text{control}} - \text{OD}_{\text{blank control}}) \times 100\%.$$

A flow cytometry assay was also conducted to evaluate cytotoxicity. 4T1 or WI38 cells were seeded in a 6-well plate at a density of 1×10^6 and cultured overnight. Then, 25 μM of **VBio-Cu^{I}Cu^{II}** or **VBio-Cu^{II}** was added and incubated for 48 h. After that, the cells were stained with Annexin V/PI and analysed by flow cytometry.

Intracellular ROS assay

The generated ROS in 4T1 cells after treatment with **VBio-Cu^{I}Cu^{II}** or **VBio-Cu^{II}** was monitored by flow cytometry using a DCFH-DA fluorescent probe as the indicator. 4T1 cells were seeded in 6-well plates at a density of 1×10^6 cells and cultured overnight. Then, the cells were treated with 10.0 μM **VBio-Cu^{I}Cu^{II}**/**VBio-Cu^{II}** for 12 h. Subsequently, the cells were washed with fresh medium three times and incubated with DCFH-DA (2 μM) at 37 °C for 30 min. The collected cells were analysed for ROS levels by flow cytometry.

Cellular uptake studies

4T1 and WI38 cells were seeded in 10 mm culture dishes at a density of 1×10^6 cells. After 24 h of incubation, the cells were treated with 10 μM of **VBio-Cu^{I}Cu^{II}** for 6 h, 12 h, 24 h 36 h and 48 h, respectively. The cells were collected and lysed with nitric acid (70%, 2.5 mL) and hydrogen peroxide (30%, 1 mL). The obtained samples were diluted 100 times with deionized water, and the copper content was then quantified by ICP-MS analysis.

In vivo tumor therapy

All animal experiments were assigned to Nanjing OG Science and Technology Service Co., Ltd. BALB/c nude mice (6 weeks old) were purchased from Changzhou Cavens Laboratory Animal Co., Ltd (Changzhou, China). All animal experiments were conducted in accordance with the protocol approved by the Animal Nursing and Use Committee of Nanjing OGpharma Co., Ltd (Nanjing, China, approval no. SYXK(SU) 2017-0040). The 4T1 tumor-bearing mouse model was established by subcutaneously injecting cells (5×10^6 cells per mouse) into the rear right flank of BALB/c nude mice. Then, when the tumor volume reached approximately 100 mm^3, the mice were randomly divided into 3 groups, where each group had 6 mice. The tumor-implanted mice were injected with saline (group 1), 20 mg kg^{-1} **VBio-Cu^{I}Cu^{II}** (group 2) or 20 mg kg^{-1} **VBio-Cu^{II}** (group 3) through the tail vein every other day. The body weight and tumor size of the mice were measured every two days. The tumor size was determined by measuring the length (l) and width (w) and calculating the volume ($V = lw^2/2$). Finally, all mice were sacrificed on the 15th day and the main organs (heart, liver, spleen, lung, and kidney) were dissected for the H&E staining test.

Author contributions

Fuping Huang and Zhaoguo Hong designed, executed, and analysed experiments, and wrote and revised manuscripts. Xin You, Jingjing Zhong and Di Yao assisted in performance testing. Liangliang Zhang, Shulin Zhao, and Hong Liang provided revision guidance, suggestions and part of the financial support.

Conflicts of interest

There are no conflicts to declare.

Acknowledgements

This work was supported by the National Natural Science Foundation of China (22075056, 21861005, 21964005, and 22177022), Natural Science Foundation of Guangxi Province (no. 2019GXNSFFA245006), and the Foundation of State Key Laboratory for Chemistry and Molecular Engineering of Medicinal Resources (CMEMR2018-C15).

References

1 Q. Chen, C. Liang, X. Sun, J. Chen, Z. Yang, H. Zhao, L. Feng and Z. Liu, H_2O_2-responsive liposomal nanoprobe for photoacoustic inflammation imaging and tumor theranostics via in vivo chromogenic assay, *Proc. Natl. Acad. Sci. U. S. A.*, 2017, **114**, 5343–5348.
2 Y. Liu, Y. Jiang, M. Zhang, Z. Tang, M. He and W. Bu, Modulating Hypoxia via Nanomaterials Chemistry for Efficient Treatment of Solid Tumors, *Acc. Chem. Res.*, 2018, **51**, 2502–2511.
3 K. Poudel, K. S. Nam, J. Lim, S. K. Ku, J. Hwang, J. O. Kim and J. H. Byeon, Modified Aerotaxy for the Plug-in Manufacture of Cell-Penetrating Fenton Nanoagents for Reinforcing Chemodynamic Cancer Therapy, *ACS Nano*, 2022, **16**, 19423–19438.
4 G. Reina, J. M. Gonzalez-Dominguez, A. Criado, E. Vazquez, A. Bianco and M. Prato, Promises, facts and challenges for graphene in biomedical applications, *Chem. Soc. Rev.*, 2017, **46**, 4400–4416.
5 Z. Tang, Y. Liu, M. He and W. Bu, Chemodynamic Therapy: Tumour Microenvironment-Mediated Fenton and Fenton-like Reactions, *Angew. Chem., Int. Ed.*, 2019, **58**, 946–956.
6 E. Hwang and H. S. Jung, Metal–organic complex-based chemodynamic therapy agents for cancer therapy, *Chem. Commun.*, 2020, **56**, 8332–8341.
7 S. Kim, C. Hwang, D. I. Jeong, J. Park, H.-J. Kim, K. Lee, J. Lee, S.-H. Lee and H.-J. Cho, Nanorod/nanodisk-integrated liquid crystalline systems for starvation, chemodynamic, and photothermal therapy of cancer, *Bioeng. Transl. Med.*, 2022, e10470.

8 N. Alamer, A. Meshkini, L. Khoshtabiat and A. Behnamsani, Synergizing effects of chemodynamic therapy and chemotherapy against breast cancer by oxaliplatin-loaded polydopamine/BSA@copper ferrite, *J. Drug Delivery Sci. Technol.*, 2022, **72**, 103391.
9 Z. Hong, J. Zhong, S. Gong, S. Huang, Q. Zhong, D. Ding, H. Bian, H. Liang and F.-P. Huang, A triphenylphosphine coordinated cinnamaldehyde-derived copper(I) Fenton-like agent with mitochondrial aggregation damage for chemodynamic therapy, *J. Mater. Chem. B*, 2022, **10**, 5086–5094.
10 D. Hanahan and R. A. Weinberg, Hallmarks of Cancer: The Next Generation, *Cell*, 2011, **144**, 646–674.
11 C. Lennicke, J. Rahn, R. Lichtenfels, L. A. Wessjohann and B. Seliger, Hydrogen peroxide–production, fate and role in redox signaling of tumor cells, *Cell Commun. Signaling*, 2015, **13**, 39.
12 Y. Wang, S. Zhang, J. Wang, Q. Zhou, J. F. Mukerabigwi, W. Ke, N. Lu and Z. Ge, Ferrocene-containing polymersome nanoreactors for synergistically amplified tumor-specific chemodynamic therapy, *J. Controlled Release*, 2021, **333**, 500–510.
13 J. Li, A. Dirisala, Z. Ge, Y. Wang, W. Yin, W. Ke, K. Toh, J. Xie, Y. Matsumoto, Y. Anraku, K. Osada and K. Kataoka, Therapeutic Vesicular Nanoreactors with Tumor-Specific Activation and Self-Destruction for Synergistic Tumor Ablation, *Angew. Chem., Int. Ed.*, 2017, **56**, 14025–14030.
14 Y. Kang and K.-Y. Hwang, Effects of reaction conditions on the oxidation efficiency in the Fenton process, *Water Res.*, 2000, **34**, 2786–2790.
15 M. Chen, S. Zhao, J. Zhu, E. Feng, F. Lv, W. Chen, S. Lv, Y. Wu, X. Peng and F. Song, Open-Source and Reduced-Expenditure Nanosystem with ROS Self-Amplification and Glutathione Depletion for Simultaneous Augmented Chemodynamic/Photodynamic Therapy, *ACS Appl. Mater. Interfaces*, 2022, **14**, 20682–20692.
16 Z. Tang, P. Zhao, H. Wang, Y. Liu and W. Bu, Biomedicine Meets Fenton Chemistry, *Chem. Rev.*, 2021, **121**, 1981–2019.
17 J. D. Martin, H. Cabral, T. Stylianopoulos and R. K. Jain, Improving cancer immunotherapy using nanomedicines: progress, opportunities and challenges, *Nat. Rev. Clin. Oncol.*, 2020, **17**, 251–266.
18 H. Yuan, L. Zhang, T. Ma, J. Huang, C. Nie, S. Cao, X. Xiang, L. Ma, C. Cheng and L. Qiu, Spiky Cascade Biocatalysts as Peroxisome-Mimics for Ultrasound-Augmented Tumor Ablation, *ACS Appl. Mater. Interfaces*, 2022, **14**, 15970–15981.
19 T. Xue, C. Xu, Y. Wang, Y. Wang, H. Tian and Y. Zhang, Doxorubicin-loaded nanoscale metal–organic framework for tumor-targeting combined chemotherapy and chemodynamic therapy, *Biomater. Sci.*, 2019, **7**, 4615–4623.
20 Q. Tian, F. Xue, Y. Wang, Y. Cheng, L. An, S. Yang, X. Chen and G. Huang, Recent advances in enhanced chemodynamic therapy strategies, *Nano Today*, 2021, **39**, 101162.
21 N. Muhammad, N. Sadia, C. Zhu, C. Luo, Z. Guo and X. Wang, Biotin-tagged platinum(IV) complexes as targeted cytostatic agents against breast cancer cells, *Chem. Commun.*, 2017, **53**, 9971.
22 B. Luo, L. Chen, Z. Hong, X. You, F.-P. Huang, H.-D. Bian, L. Zhang and S. Zhao, A simple and feasible atom-precise biotinylated Cu(I) complex for tumor-targeted chemodynamic therapy, *Chem. Commun.*, 2021, **57**, 6046.
23 S. Maiti and P. Paira, Biotin conjugated organic molecules and proteins for cancer therapy: A review, *Eur. J. Med. Chem.*, 2018, **145**, 206–223.
24 S. Paul, P. Kundu, P. Kondaiah and A. R. Chakravarty, BODIPY-Ruthenium(II) Bis-Terpyridine Complexes for Cellular Imaging and Type-I/-II Photodynamic Therapy, *Inorg. Chem.*, 2021, **60**, 16178–16193.
25 J. D. Schneider, B. A. Smith, G. A. Williams, D. R. Powell, F. Perez, G. T. Rowe and L. Yang, Synthesis and Characterization of Cu(II) and Mixed-Valence Cu(I)Cu(II) Clusters Supported by Pyridylamide Ligands, *Inorg. Chem.*, 2020, **59**, 5433–5446.
26 S. Chen, X. Zhao, J. Chen, J. Chen, L. Kuznetsova, S. S. Wong and I. Ojima, Mechanism-based tumor-targeting drug delivery system. Validation of efficient vitamin receptor-mediated endocytosis and drug release, *Bioconjugate Chem.*, 2010, **21**, 979–987.
27 L. Reguera, A. Cano, J. Rodríguez-Hernández, D. G. Rivera, E. V. Van der Eycken, D. Ramírez-Rosales and E. Reguera, $Cu^{I}Cu^{II}$ and Ag^{I} p-isocyanobenzoates as novel 1D semiconducting coordination oligomers, *Dalton Trans.*, 2020, **49**, 12432.
28 P. Liu and E. J. M. Hensen, Highly Efficient and Robust Au/$MgCuCr_2O_4$ Catalyst for Gas-Phase Oxidation of Ethanol to Acetaldehyde, *J. Am. Chem. Soc.*, 2013, **135**, 14032.
29 T. Soltani and B.-K. Le, Enhanced formation of sulfate radicals by metal-doped $BiFeO_3$ under visible light for improving photo-Fenton catalytic degradation of 2-chlorophenol, *Chem. Eng. J.*, 2017, **313**, 1258.
30 Z. Tang, P. Zhao, H. Wang, Y. Liu and W. Bu, Biomedicine Meets Fenton Chemistry, *Chem. Rev.*, 2021, **121**, 1981–2019.
31 C. Wang, F. Cao, Y. Ruan, X. Jia, W. Zhen and X. Jiang, Specific Generation of Singlet Oxygen through the Russell Mechanism in Hypoxic Tumors and GSH Depletion by Cu-TCPP Nanosheets for Cancer Therapy, *Angew. Chem., Int. Ed.*, 2109, **58**, 9846–9850.
32 J. Liu, Y. Yuan, Y. Cheng, D. Fu, Z. Chen, Y. Wang, L. Zhang, C. Yao, L. Shi, M. Li, C. Zhou, M. Zou, G. Wang, L. Wang and Z. Wang, Copper-Based Metal–Organic Framework Overcomes Cancer Chemoresistance through Systemically Disrupting Dynamically Balanced Cellular Redox Homeostasis, *J. Am. Chem. Soc.*, 2022, **144**, 4799–4809.
33 A. Munoz, D. H. Petering and C. F. Shaw, Reactions of Electrophilic Reagents That Target the Thiolate Groups of Metallothionein Clusters: Preferential Reaction of the α-Domain with 5,5′-Dithio-bis(2-nitrobenzoate) (DTNB) and Aurothiomalate (AuSTm), *Inorg. Chem.*, 1999, **38**, 5655–5659.
34 R. Vinck, A. Gandioso, P. Burckel, B. Saubaméa, K. Cariou and G. Gasser, Red-Absorbing Ru(II) Polypyridyl Complexes

with Biotin Targeting Spontaneously Assemble into Nanoparticles in Biological Media, *Inorg. Chem.*, 2022, **61**, 13576–13585.

35 M. L. Alfieri, M. Massaro, M. d'Ischia, G. D'Errico, N. Gallucci, M. Gruttadauria, M. Licciardi, L. F. Liotta, G. Nicotra, G. Sfuncia and S. Riela, Site-specific halloysite functionalization by polydopamine: A new synthetic route for potential near infrared-activated delivery system, *J. Colloid Interface Sci.*, 2022, **606**, 1779–1791.

36 G. M. Sheldrick, SHELXT-Integrated Space-Group and Crystal-Structure Determination, *Acta Crystallogr., Sect. A: Found. Adv.*, 2015, **71**, 3–8.

37 O. V. Dolomanov, L. J. Bourhis, R. J. Gildea, J. A. K. Howard and H. Puschmann, OLEX2: a complete structure solution, refinement and analysis program, *J. Appl. Crystallogr.*, 2009, **42**, 339–341.

38 G. Sheldrick, Crystal structure refinement with SHELXL, *Acta Crystallogr., Sect. C: Struct. Chem.*, 2015, **71**, 3–8.